CrossMark

Plasmonic effect of silver nanoparticles intercalated into mesoporous betalain-sensitized-TiO$_2$ film electrodes on photovoltaic performance of dye-sensitized solar cells

Kasim U. Isah[1] [ID] · Bukola J. Jolayemi[1] · Umaru Ahmadu[1] · Mohammed Isah Kimpa[1] ·
Noble Alu[2]

Abstract Dye-sensitized solar cells (DSSCs) comprising mesoporous TiO$_2$ films and betalain pigments extracted from red *Bougainvillea glabra* flower as natural dye sensitizers were fabricated and enhanced by the intercalation of the plasmonic silver nanoparticles (Ag NPs) into the pores of mesoporous TiO$_2$ electrodes by successive ionic layer adsorption and reaction (SILAR) method. The TiO$_2$/ Ag NPs composite films were characterized by SEM and UV–Vis spectroscopy. I–V characteristics of the devices were measured by solar simulator (AM1.5 at 100 mW/ cm^2). The incorporation of the Ag nanoparticles into the pores of mesoporous TiO$_2$ electrodes with one SILAR deposition cycle of the Ag NPs produced the best plasmonic enhanced-DSSC giving a short-circuit current density (J_{sc}), fill factor (FF), and power conversion efficiency (PCE) of 1.01 mA cm^{-2}, 0.77, and 0.27 %, respectively. This development amounts to 50 % efficiency enhancement over the reference DSSC that had a short-circuit current density (J_{sc}), fill factor (FF), and power conversion efficiency (PCE) of 0.7 mA cm^{-2}, 0.57, and 0.18 %, respectively.

Keywords Plasmonic · Silver nanoparticles · SILAR · DSSCs · Betalain · *Bougainvillea glabra*

✉ Kasim U. Isah
kasim309@futminna.edu.ng

[1] Department of Physics, School of Physical Sciences, Federal University of Technology, Minna, Nigeria

[2] Physics Advanced Laboratory (PAL), Sheda Science and Technology Complex (SHESTCO), Abuja, Nigeria

Introduction

Dye-sensitized solar cells (DSSCs) have remained one of the most promising choices for the realization of low-cost solar cells; it has, in the recent years, attracted remarkable attention owing to simplicity of its fabrication process and low manufacturing cost with excellent light absorbing materials [1–3]. Nevertheless, the power conversion efficiency (PCE) of the device has barely gone up to 11.9 % [4]. Many technological innovations have been developed to improve the efficiency and, at the same time, to reduce the cost of production ranging from interfacial modification [5, 6] to material choice and engineering [7]. This development leads to the consideration of natural dyes from plant sources which are cost-effective, non-toxic, and completely biodegradable compared with the much expensive and toxic synthesized counterparts based on metal complex-like ruthenium (II) and metal-free like porphyrin [8]. Betalain has been regarded by many researchers to be a most promising candidate of choice out of the three most exploited dye pigments from plant sources: chlorophylls, anthocyanins, and betalains [9]. Conversely to the anthocyanins, betalains possess essential functional groups (–COOH) to anchor better to the TiO$_2$ nanoparticles than the functional groups (–OH) present in anthocyanins [10–13]. Indeed, the interaction between TiO$_2$ film and carboxylic functions should bring a stronger electronic coupling and rapid forward and reverse electron transfer reactions [9].

Also, the incorporation of plasmonic metal nanoparticles (NPs) into the electrode (usually m-TiO$_2$) of dye-sensitized solar cells (DSSCs) to boost the light absorption due to their localized surface plasmon (LSP) effect has been very outstanding [14–17]. Noble plasmonic metal nanostructures, such as gold (Au), silver (Ag) [18, 19],

Springer

aluminum (Al) [20], their alloys [16], and their core–shell formation [21–25], have been incorporated into DSSCs to effectively utilize the incident photon and improve cell performance. Many methods, both chemical and physical categories, including, wet chemical [26], polyol process [27], seed-mediated growth [28], photochemical [29], sonochemical [30], electrochemical [31], bioinspired [32], sputtering [33], and laser ablation [34], which have been, hitherto, reportedly employed to synthesize various plasmonic Ag nanostructures, possess one disadvantage or the other, such as toxic reducing agents, impurities, organic solvents, or may require special condition like high-temperature or low-pressure environment, and sometimes expensive and time-consuming procedures may be involved [35].

Successive ionic layer adsorption and reaction (SILAR) method was used in this work for the intercalation of Ag nanoparticles into the pores of mesoporous TiO_2 photoelectrodes of betalain-sensitized DSSCs. It offers simple, inexpensive, and time-saving procedures, which can be carried out at room temperature with no restrictions on substrate material, dimensions or its surface profile, and the thickness of the film or nanoparticle can be easily controlled [36–38].

Experimental

Preparation of photosensitizer

The photosensitizer was made of natural dye from betalain pigments extracted from red *Bougainvillea glabra* flower. 13.12 g of the fresh flowers was ground and well blended together in 100 ml of distilled water in an electric blender. Then, the mixture was filtered, and the filtrate was used as the sensitizing dye without further purification.

Preparation of active electrode layer

Fluorine-doped tin oxide (FTO: TCO30-8 glass, 8 Ω/sq, 3 mm thick, Solaronix) glass sheets were cleaned with detergent (sodium lauryl sulfate), rinsed with distilled water, ethanol, and dried under compressed hot air for 7 min at 70 °C in a clean container. 0.5×0.6 cm^2 area compact TiO_2 (c-TiO_2) paste (Ti-Nanoxide BL/SP, Solaronix) was screen-printed on three 2.5×2.5 cm^2 FTO glass substrates using a 70 mesh screen to obtain about 50-nm thick TiO_2 film. The film was sintered on the hotplate at 500 °C for 50 min and was allowed to slowly cool down to room temperature. Afterward, mesoporous TiO_2 (m-TiO_2) paste (Ti-Nanoxide T300/SP, Solaronix) was screen-printed on the 0.30 cm^2 of as-deposited c-TiO_2

substrates obtaining about 3.5 μm with polyester mesh screen-120. After drying at 55 °C for 30 min, the electrodes were sintered at 450 °C for 30 min, and then gradually cooled down to room temperature.

Synthesis and incorporation of silver nanoparticles

Silver nanoparticles (Ag NPs) were prepared by successive ionic layer adsorption and reaction (SILAR) method. The cationic precursor for Ag NPs using SILAR method was diamine silver complex $\left(\left[Ag(NH_3)_2 \right]^+_{(aq)} \right)$ solution. This solution was prepared using 0.35 g of $AgNO_3$ (BDH) in 200 ml of distilled water, to this, ammonia solution (NH_3OH) (ca. 33 wt% NH, Grifflin and George) was added drop by drop until colorless solution was observed. The anionic (reducing agent) solution was prepared by adding 2 ml of concentrated HCl (36 %, Loba Chemie) to 2 g of stannous chloride ($SnCl_2.2H_2O$) (BDH) in 640 ml of distilled water.

To intercalate the Ag NPs into the mesoscopic TiO_2 electrodes, the prepared electrode was immersed in the diamine silver complex $\left(\left[Ag(NH_3)_2 \right]^+_{(aq)} \right)$ solution for 2 min (adsorption), then rinsed with distilled water for 1 min (to remove excess adsorbed ions from the diffusion layer), the electrode was then transferred to the stannous chloride solution for 2 min (reduction reaction), and hence, film turns brownish due to the reduction from Ag^+ to Ag; it was then treated with acid rinse by immersing it in 0.25 M of HCl (36 %, Loba Chemie) for 30 s (to etch any loosely silver nanoparticles) and finally rinsed with distilled water for 30 s to remove the excess and unreacted species and reaction by-product from the diffusion layer. The deposition process is shown in Fig. 1.

This process was repeated for another electrode with two SILAR cycles. As soon as the required number of cycles was complete, the film was returned to the silver diamine complex solution for 30 s to form a layer of protective oxidized Ag shell on the film and rinsed in distilled water for another 30 s before drying at 100 °C in an open air until it was fully dried; this leads to the formation of a thin silver oxide shell on the film to protect the Ag nanoparticles from the iodic electrolyte [16]. To further protect the Ag NPs from the corrosive electrolyte, the films were refluxed in 0.1-M titanium (IV) isopropoxide (Sigma-Aldrich) in isopropanol solution for 25 min to form silver–titanium dioxide core–shell (Ag@TiO_2) nanoparticles and sintered at 350 °C for 20 min. The preparation process is shown in Fig. 2.

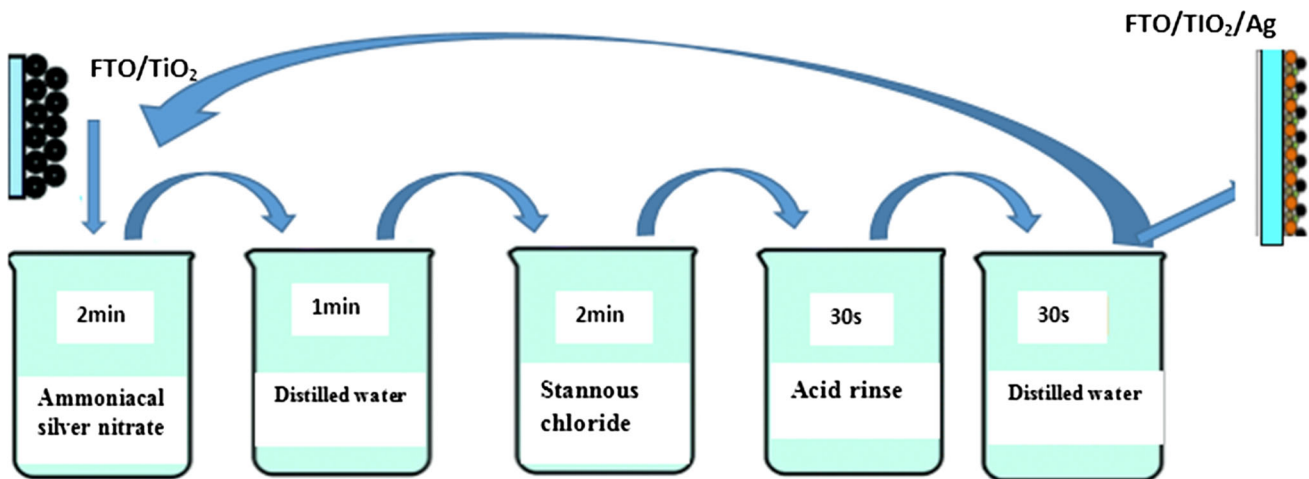The chemical reaction mechanism for the formation of Ag NPs is given in the following.

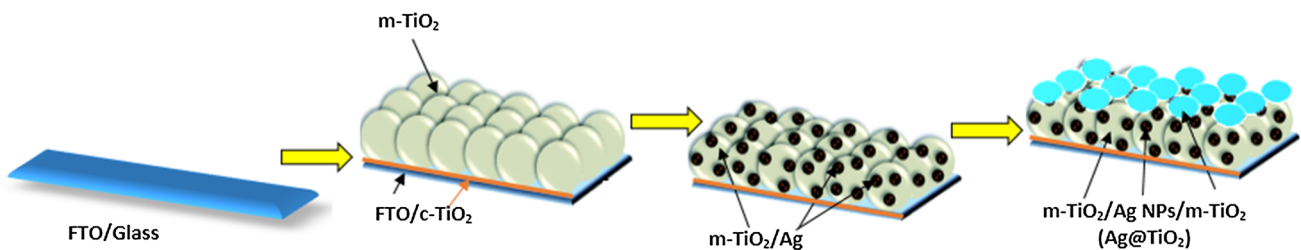**Fig. 1** Scheme of SILAR cycle process of Ag nanoparticles deposition for DSSC application


Fig. 2 Schematic of plasmonic photoanode preparation process

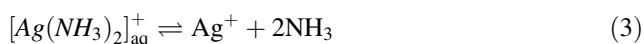*Cationic precursor (adsorption step)*

Diammine silver complex cationic precursor is obtained by adding enough ammonia solution ($NH_4OH_{(aq)}$) to $AgNO_{3(aq)}$. Brownish precipitate appears when a small amount of ammonia solution is added as a result of the formation of silver (I) oxide ($Ag_2O_{(s)}$):

$$2AgNO_{3(aq)} + 2NH_4OH_{(aq)} \rightarrow Ag_2O_{(s)} + 2NH_4NO_{3(aq)} + H_2O_{(l)} \tag{1}$$
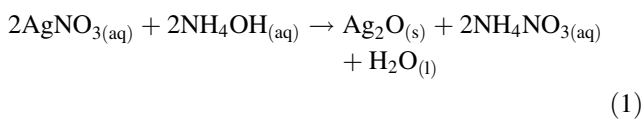
The precipitate ($Ag_2O_{(s)}$) dissolves in excess ammonia solution to form colorless diammine silver complex ion:

$$Ag_2O_{(s)} + 4NH_3 + H_2O_{(l)} \rightarrow 2\left[Ag(NH_3)_2\right]^+_{(aq)} + 2OH^-_{(aq)} \tag{2}$$
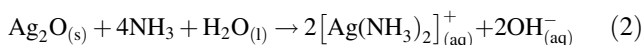
The ionic equation of the complex ion is given as:

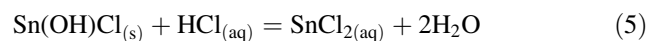$$[Ag(NH_3)_2]^+_{aq} \rightleftharpoons Ag^+ + 2NH_3 \tag{3}$$

Anionic precursor (reaction step)

Tin (II) chloride dissolves in less than its own mass of water to form insoluble tin hydroxy chloride specie in a reversible hydrolysis,
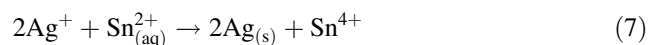
$$SnCl_2 + H_2O \rightleftharpoons Sn(OH)Cl_{(s)} + HCl_{(aq)} \tag{4}$$
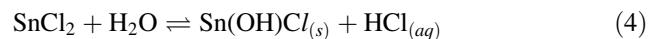
a clear solution of $SnCl_{2(aq)}$ requires addition of excess HCl

$$Sn(OH)Cl_{(s)} + HCl_{(aq)} = SnCl_{2(aq)} + 2H_2O \tag{5}$$

where

$$SnCl_{2(aq)} \rightarrow Sn^{2+} + 2Cl^- \tag{6}$$

Ag^+ is, reduced to Ag when the films were immersed in the anionic solution containing $Sn^{2+}_{(aq)}$ as follows:

$$2Ag^+ + Sn^{2+}_{(aq)} \rightarrow 2Ag_{(s)} + Sn^{4+} \tag{7}$$

Sensitization of photoanode

The bare mesoscopic TiO_2 electrode and mesoscopic TiO_2 electrodes intercalated with Ag NPs (one and two SILAR cycles) were each soaked in three different Petri dishes containing the sensitizing dye for about 20 h. After which, the dye impregnated photoanodes were then rinsed with ethanol (99 %, Sigma-Aldrich), to remove excess dye particles that were not properly adsorbed.

Fabrication of DSSCs

The counter electrodes were first prepared by screen-printing a $0.5 \times 0.6\text{-cm}^2$ thin film of platinum (Pt) paste (Platisol T/SP, Solaronix) on a bare $2.5 \times 2.5\text{-cm}^2$ FTO glass substrate, and then sintered at 450 °C for 30 min and allowed to slowly cool to room temperature.

A sandwich-type DSSCs were fabricated by assembling the dye-impregnated photoelectrodes and counter electrodes in an overlapping manner, so as to establish electrical connection between the cells and the photovoltaic measurement equipment. The assembling was achieved using hot-melt sealing gasket of Surlyn-based polymer sheet (SX1170-25PF, Solaronix) and sealed on a heating stage leaving a pinhole for the electrolyte injection for a few seconds. Finally, the iodine-based liquid electrolyte (iodolyte) was injected using micropipette before sealing with the hot-melt sealing gasket.

Characterizations

UV/Vis spectrophotometer (UV752N, Axiom) was used to measure the optical absorption spectra of the electrode film samples. The measurement was designed to cover the visible region of the electromagnetic spectrum. Scanning electron microscope (SEM) (MEL-30000, SCOTECH) was employed to record cross-sectional micrographs of the TiO_2/Ag NPs films. Also, I–V measurements were performed using a solar simulator (Keithley 4200-SCS) under simulated AM 1.5 sunlight at an irradiance of 100 mW/cm^2.

The photovoltaic parameters: maximum power output (P_{max}), fill factor (FF), and conversion efficiency (η) of the devices were evaluated according to the following formula relationship based on J–V characteristic curves:

$$P_{max} = V_{max} \times J_{max} \tag{8}$$

$$\text{Fill factor (FF)} = \frac{P_{max}}{V_{oc}J_{sc}} = \frac{V_{max}J_{max}}{V_{oc}J_{sc}} \tag{9}$$

$$\text{Efficiency } (\eta) = \frac{FF \times V_{oc} \times J_{sc}}{P_{in}} \times 100 \tag{10}$$

Results and discussions

Scanning electron microscopy (SEM)

SEM images of the bare TiO_2 and the TiO_2/Ag NPs composite films with different SILAR cycles are shown in Fig. 3. The SEM images reveal a random two-dimensional array of Ag NPs with a very broad particle size distribution. Figure 3a is the bare TiO_2 electrode, which shows the absence of Ag NPs, while Fig. 3b, c confirms the intercalation of Ag NPs in the pores of TiO_2 with one and two SILAR cycles, respectively.

The morphology of the films appears to be different, which can be attributed to the varied SILAR deposition cycles of the Ag NPs. The image of the pure TiO_2 film in Fig. 3a shows a dense surface, and there are no shinning particles observed. Considering heavy elements like Ag, they backscatter electrons more strongly than light elements like O and Ti [39], so the metallic silver appears brighter in the image as observed in Fig. 3b, c. At one SILAR cycle, the shining Ag nanoparticles are well dispersed with smaller Ag nanoparticles and more uniformly distributed in the pores of TiO_2, as shown in Fig. 3b. Conversely, for higher two SILAR deposition cycles of Ag NPs, the Ag nanoparticles became gradually aggregated to form bigger Ag NPs as observed in Fig. 3c.

UV–Vis spectroscopy

Absorption spectra of a dye reflect optical transition probability between the ground state, the excited state, and the solar energy range absorbed by the dye [13]. The comparative optical spectra of the pure betalain dye extract, betalain dye extract adsorbed into TiO_2 (TiO_2/dye) electrode, TiO_2/Ag NPs (one cycle)/dye, and TiO_2/Ag NPs (two cycles)/dye are shown in Fig. 4.

The betalain dye adsorbed into TiO_2 (TiO_2/dye) electrode shows a reduced absorbance compared with that of betalain dye extract only, as shown in Fig. 4a. The betalain extract shows a broad absorption spectrum in the visible
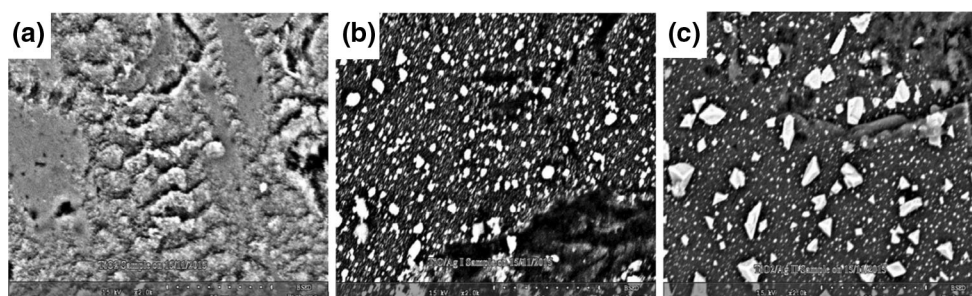

Fig. 3 SEM images of **a** bare TiO_2, **b** TiO_2/Ag NPs one SILAR cycle, and **c** TiO_2/Ag NPs two SILAR cycles

Fig. 4 Comparison of absorption spectra of pure betalain dye extract in solution with **a** betalain dye extract adsorbed on TiO$_2$, **b** dye extract adsorbed on TiO$_2$/Ag NPs (one cycle), and **c** betalain dye extract adsorbed on TiO$_2$/Ag NPs (two cycles)
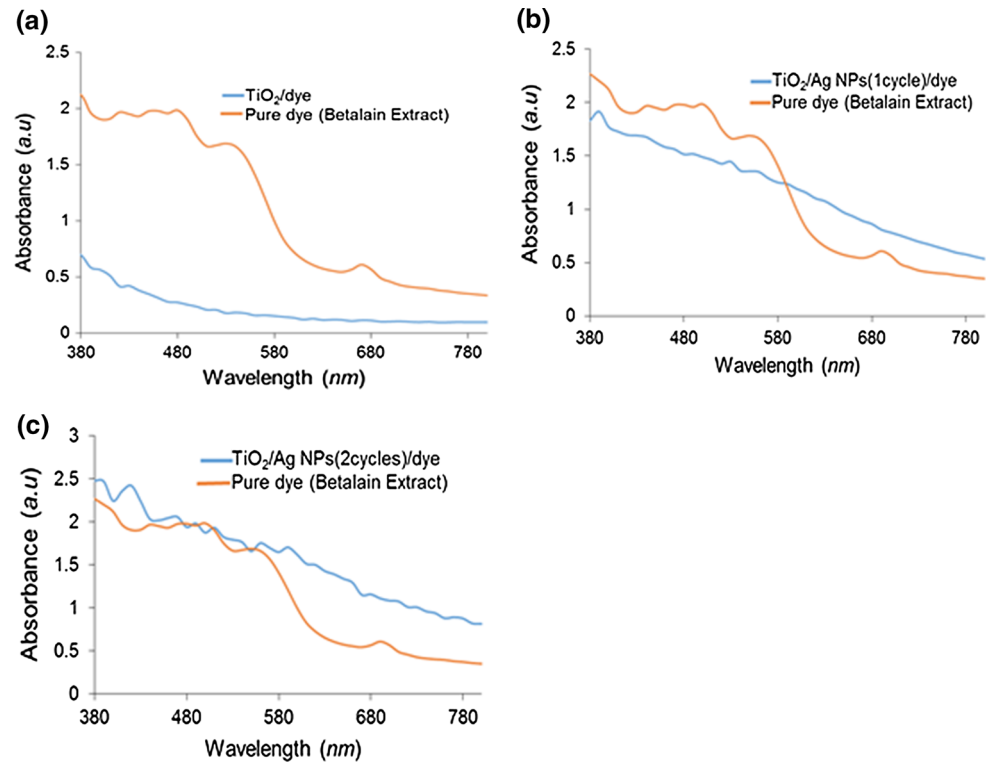
Fig. 5 Absorption spectra of **a** TiO$_2$/Ag NPs films of one and two SILAR deposition cycles and **b** dye impregnated TiO$_2$/Ag NPs films of one and two SILAR deposition cycles on soda lime glass substrate
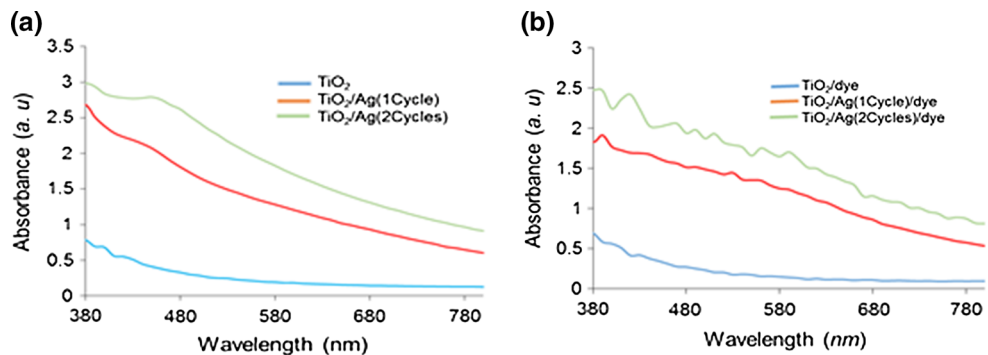
light region (ca. 400–700 nm) indicating that betalain has the ability to function as an efficient sensitizer for wide bandgap semiconductors [40, 41]. Three absorption peaks at about 480, 535, and 670 nm are observed, which are ascribed to the betalain pigments present in the dye [42].

Figure 4b, c shows synergistic absorption spectra of dye and Ag NPs on TiO$_2$ electrode with one and two SILAR cycles, respectively, both of which show higher absorption intensity compared with TiO$_2$/dye only in Fig. 4a. This suggests that the incorporation of Ag NPs with one and two SILAR cycles has significantly improved the optical absorption of the electrode which is attributable to localized surface plasmons (LSP) effect of the nanoparticles. The two SILAR cycles show the highest absorption intensity indicating the presence of more Ag NPs, which couple with the dye to increase the optical absorption for

the electrode with two SILAR cycles. A single absorption peak around 390 nm could be detected with an additional shoulder at 530 nm from Fig. 4b. In addition to the peaks detected in (b), there are other additional absorption peaks around 420, 470, 490, 510, 560, and 590 nm in (c).

The comprehensive comparison of optical absorption spectra of bare, incorporated Ag-TiO$_2$, and impregnated TiO$_2$/Ag/dye films on soda lime glass substrate is shown in Fig. 5, before and after dye sensitizer adsorption.

The absorption spectra of TiO$_2$ film with Ag nanoparticles (TiO$_2$–Ag NPs), as shown in Fig. 5a, show broad peaks centered at 450 nm for both one and two SILAR deposition cycles, which is attributable to localized surface plasmons (LSP) effect and their intensities increase as more Ag NPs are loaded onto TiO$_2$ from one to two SILAR cycles. This result indicates the excitation of LSP on the

Springer

TiO_2–Ag NPs. TiO_2 film with both Ag nanoparticles and dye (TiO_2/Ag NPs/dye) in Fig. 5b shows lower absorption intensities for one and two SILAR deposition cycles compared with that of Fig. 5a. This result indicates that Ag nanoparticles incorporation clearly enhances the photon harvesting ability of TiO_2 adsorbed with dye.

Device performance efficiency

The current density–voltage (J–V) and power density–voltage (P–V) characteristics were measured to study the photoelectric performances of both the bare and incorporated plasmonic Ag nanoparticles (Ag NPs) dye-sensitized solar cells (DSSCs).

Figure 6 shows the J–V and P–V characteristic curves of both the bare and intercalated plasmonic Ag NPs DSSCs. The photovoltaic performances of the cells are determined through the photovoltaic parameters (short-circuit current density (J_{sc}), open-circuit voltage (V_{oc}), fill factor (FF), and conversion efficiency (η), which are obtained from the J–V and P–V characteristic curves of the cells. The fill factor (FF) defined as the ratio of P_{max} and the product $J_{sc} \cdot V_{oc}$ shows curve squareness, and the closer to unity the fill factor is, the better cell quality will be [43].

The photovoltaic performance parameters: short-circuit current (J_{sc}), open-circuit voltage (V_{oc}), fill factor (FF), and conversion efficiency (η) of the cells, are shown in Table 1.

As it has been reported that the surface plasmon effect is caused by light-driven collective oscillations of conduction electrons in metallic nanoparticles, the nanoparticles must be smaller than the wavelength of exciting light for electrons to oscillate with the electric field of light. When these conditions are met, an enhanced electromagnetic field is found nearby the surface of nanoparticles. The enhanced electromagnetic field is highly dependent upon the wavelength of incident light, as well as the shape, size, and aggregation state of the nanoparticles [44].

Thus, it is observed, both plasmonic Ag NPs incorporated DSSCs experience an improvement in their respective photocurrent densities (J_{sc}) with the cell with one SILAR cycle showing better enhancement from plasmonic effect. The generated photocurrent density (J_{sc}) increases with the introduction of Ag NPs, which is found to be 44 and 19 % higher than the reference device (device 1) for one and two SILAR cycles, respectively, as shown in Table 1; thus, showing the electron transport efficiency in the TiO_2/dye/electrolyte interface is improved. With the increase in the amount of incorporated Ag NPs, increase in the recombination probability arises and leads to the decline of photocurrent density [20] and, as a result, reduces the PCE of the DSSCs when the SILAR cycles increased from one to two. Considering the size and aggregation state of Ag NPs as observed in Fig. 3 of SEM analysis, these generate defects at the surface of the active layer of the cell. These defects are potential recombination centers which are capable of trapping generated carriers, and thus, the surface recombination pose a negative impact on the effective carrier lifetime and, subsequently, on the

Fig. 6 J–V and P–V characteristic curves of **a** DSSC with bare TiO_2 electrode, **b** DSSC with one SILAR cycle TiO_2 intercalated Ag NPs electrode, and **c** DSSC with two SILAR cycles TiO_2 intercalated Ag NPs electrode
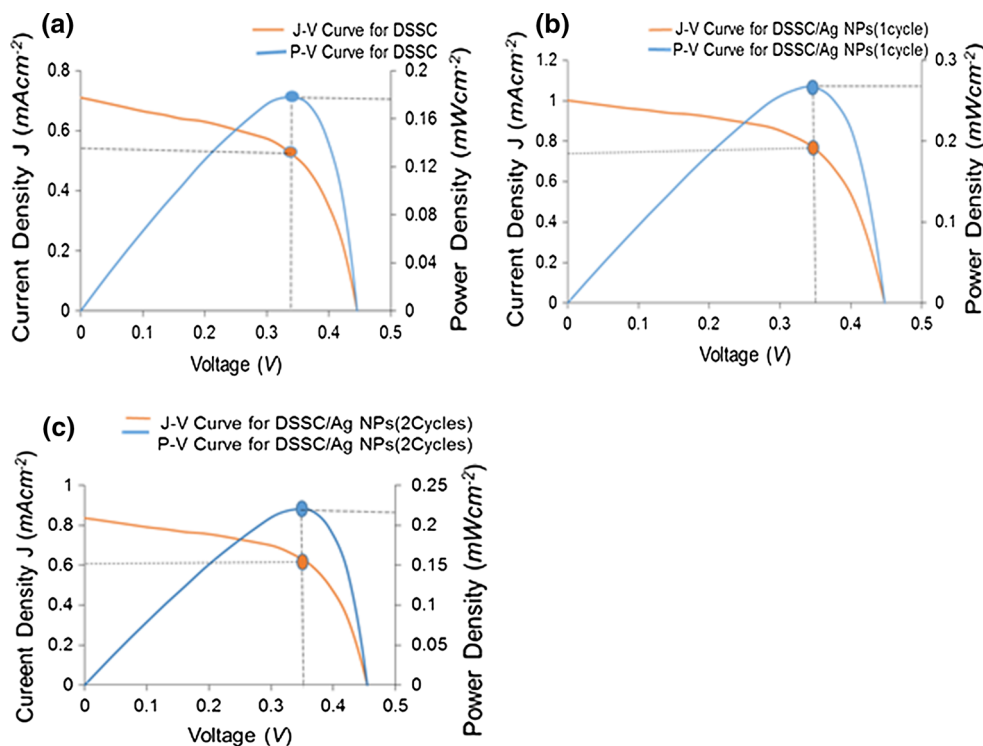
Table 1 Photovoltaic parameters of plasmonic-DSSC

Device	Photoanode	J_{sc} (mA cm^{-2})	V_{oc} (V)	J_{max} (mA cm^{-2})	V_{max} (V)	FF	η (%)	% Increase in η
1	TiO$_2$ (bare)	0.70	0.45	0.53	0.34	0.57	0.18	0
2	TiO$_2$/Ag (one cycle)	1.01	0.45	0.77	0.35	0.59	0.27	50
3	TiO$_2$/Ag (two cycles)	0.83	0.45	0.60	0.37	0.59	0.22	22

efficiency of the solar cells [21, 32, 44–46]. Also, the recombination reaction creates an internal short-circuit throughout the bulk of the photoanode layer [32]; as a result, the device shows a lower PCE with two SILAR cycles. Also, the scattering effect may contribute to the decline, but the plasmonic effect still dominates because of the relatively small size of the nanoparticles [20].

The efficiency of the plasmonic-DSSC (device 2) obtained with one SILAR deposition cycle of Ag NPs onto the TiO$_2$ photoelectrode is 0.27 % indicating an improvement of 50 % compared with the efficiency of the reference DSSC (device 1) which had an efficiency of 0.18 %. The open-circuit voltage (V_{oc}) and fill factor (FF) remain almost unchanged, while the short-circuit current density (J_{sc}) indicates a clear increase owed to the light trapping as a result of LSP effect of Ag NPs, which make more photons ready and available for dyes to absorb for photoelectrons generation. The intercalation of Ag nanoparticles has been shown not to significantly affect the values of V_{oc}, because V_{oc} is determined mainly by the redox potential and the Fermi energy of semiconductors and is not significantly affected with the change in size of the Ag NPs [18, 47, 48].

Conclusion

The DSSCs comprising mesoporous TiO$_2$ films and natural betalain dye extract from red *Bougainvillea glabra* flower as photosensitizers were prepared and enhanced by the intercalation of the Ag nanoparticles into the TiO$_2$ electrodes by successive ionic layer adsorption and reaction (SILAR) method. The morphological and optical characteristics of TiO$_2$/Ag composite films were determined using SEM and UV–Vis spectrophotometer, respectively. The intercalation of plasmonic Ag nanostructures increased the optical absorption of the photoanodes over a wide range of wavelengths. The reference DSSC had a short-circuit current density (J_{sc}) and power conversion efficiency (PCE) of 0.70 mA cm^{-2} and 0.18 %, respectively, while the cell with two SILAR Ag NPs incorporated into photoelectrode had a short-circuit current density (J_{sc}) and power conversion efficiency (PCE) of 0.83 mA cm^{-2} and 0.22 %, respectively, representing a 22 % enhancement in efficiency. The intercalation of the Ag nanoparticles into the TiO$_2$ electrodes with one SILAR deposition cycle produced the best plasmonic-DSSC cell performance with the maximum short-circuit current density (J_{sc}) and PCE of 1.01 mA cm^{-2} and 0.27 %, respectively. This shows a significant improved power conversion efficiency of 50 % with one SILAR deposition cycle of Ag NPs intercalated into the photoanode over the bare photoanode reference DSSC cell.

References

1. Adhyaksa, G.W.P., Baek, S., Lee, G.I., Lee, D.K., Lee, J.-Y., Kang, J.K.: Coupled near- and far-field scattering in silver nanoparticles for high-efficiency, stable, and thin plasmonic dye-sensitized solar cells. ChemSusChem **7**, 2461–2468 (2014)

2. Pan, M., Huang, N., Zhao, X., Fu, J., Zhong, X.: Enhanced efficiency of dye-sensitized solar cell by high surface area anatase-TiO$_2$-Modified P25 paste. J. Nanomater. **760685B**, 1–6 (2013). doi:10.1155/2013/760685

3. Luque, A., Mart, A.: Increasing the efficiency of ideal solar cells by photon induced transitions at intermediate levels. Phys. Rev. Lett. **78**, 5014–5017 (1997). doi:10.1103/PhysRevLett.78.5014

4. NREL: Best Research-Cell Efficiencies. National Renewable Energy Laboratory (NREL) (2015). http://www.nrel.gov/ncpv/images/efficiency_chart.jpg. Accessed 30 Dec 2015

5. Ma, B.B., Gao, R., Wang, L.D., Zhu, Y.F., Shi, Y.T., Geng, Y., Dong, H.P., Qiu, Y.: Recent progress in interface modification for dye-sensitized solar cells. Sci. China Chem. **53**, 1669–1678 (2010)

6. Wu, K.-W., Tedla, A., Mua, Y.-T., Tai, Y.: Interfacial modification of the working electrode of dye-sensitized solar cells to improve the charge transport properties. J. Mater. Chem. A **1**, 12137–12143 (2013). doi:10.1039/C3TA12027A

7. Suhaimi, S., Shahimin, M.M., Alahmed, Z.A., Chyský, J., Reshak, A.H.: Materials for Enhanced dye-sensitized solar cell performance: electrochemical application. Int. J. Electrochem. Sci. **10**, 2859–2871 (2015)

8. Zhou, H., Wu, L., Gao, Y., Ma, T.: Dye-sensitized solar cells using 20 natural dyes as sensitizers. J. Photochem. Photobiol. A Chemistry **291**, 188–194 (2011). doi:10.1016/j.jphotochem.2011.02.008

9. Calogero, G., Yumb, J.-H., Sinopoli, A., Marco, G.D., Gratzel, M., Nazeeruddin, M.K.: Anthocyanins and betalains as light-

harvesting pigments for dye-sensitized solar cells. Sol. Energy **86**, 1563–1575 (2012). doi:10.1016/j.solener.2012.02.018

10. Calogero, G., Di Marco, G., Cazzanti, S., Caramori, S., Argazzi, R.D.C.A., Bignozzi, C.: Efficient dye-sensitized solar cells using red turnip and purple wild sicilian prickly pear fruits. Int. J. Mol. Sci. **11**, 254–267 (2010). doi:10.3390/ijms11010254

11. Quin, C., Clark, A.: DFT characterization of the optical and redox properties of natural pigments relevant to dye-sensitized solar cells. Chem. Phys. Lett. **438**, 26–30 (2007)

12. Zhang, D., Lanier, S.M., Downing, J.A., Avent, J.L., Lum, J., McHale, J.L.: Betalain pigments for dye-sensitized solar cells. J. Photochem. Photobiol. A Chem. **195**, 72–80 (2008)

13. Isah, K.U., Ahmadu, U., Idris, A., Kimpa, M.I., Uno, U.E., Ndamitso, M.M., Alu, N.: Betalain pigments as natural photosensitizers for dye-sensitized solar cells: the effect of dye pH on the photoelectric parameters. Mater. Renew. Sustain. Energy **4**, 1–5 (2015). doi:10.1007/s40243-014-0039-0

14. Jing, H., Zhang, L., Wang, H.: Geometrically tunable optical properties of metal nanoparticles. In: Kumar, C. (Eds.) UV-VIS and Photoluminescence Spectroscopy for Nanomaterials Characterization, pp. 1–74. Springer, Berlin Heidelberg, Germany (2013). doi:10.1007/978-3-642-27594-4

15. Hou, W., Cronin, S.B.: A review of surface plasmon resonance-enhanced photocatalysis. Adv. Funct. Mater. **23**, 1612–1619 (2013). doi:10.1002/adfm.201202148

16. Xu, Q., Liu, F., Liu, Y., Cui, K., Feng, X.Z.W., Huang, Y.: Broadband light absorption enhancement in dye-sensitized solar cells with Au–Ag alloy popcorn nanoparticles. Sci. Rep. **3**, 1–7 (2013). doi:10.1038/srep02112

17. Zhou, N., López-Puente, V., Wang, Q., Polavarapu, L., Pastoriza-Santos, I., Xu, Q. H.: Plasmon-enhanced light harvesting: applications in enhanced photocatalysis, photodynamic therapy and photovoltaics. RSC Adv. **5**, 29076–29097 (2015). doi:10.1039/C5RA01819F

18. Photiphitak, C., Rakkwamsuk, P., Muthitamongkol, P., Sae-Kung, C., Thanachayanont, C.: Effect of silver nanoparticle size on efficiency enhancement of dye-sensitized solar cells. Int. J. Photoenergy **258635**, 1–8 (2011). doi:10.1155/2011/258635

19. Lin, S.-J., Lee, K.-C., Wu, J.-L., Wu, J.-Y.: Enhanced performance of dye-sensitized solar cells via plasmonic sandwiched structure. Appl. Phys. Lett. **99**, 1–3 (2011). doi:10.1063/1.3616139

20. Xu, Q., Liu, F., Liu, Y., Meng, W., Cui, K., Feng, X., Zhang, W., Huang, H.: Aluminum plasmonic nanoparticles enhanced dye sensitized solar cells. Opt. Express **22**, A301–A310 (2014). doi:10.1364/OE.22.00A301

21. Brown, M.D., Suteewong, T., Kumar, R.S.S., D'Innocenzo, V., Petrozza, A., Lee, M.M., Wiesner, U., Snaith, H.J.: Plasmonic dye-sensitized solar cells using core—shell metal—insulator nanoparticles. Nano Lett. **11**, 438–445 (2010). doi:10.1021/nl1031106

22. Qi, J., Dang, X., Hammond, P.T., Belcher, A.M.: Highly efficient plasmon-enhanced dye-sensitized solar cells through metal@oxide core-shell nanostructure. ACS Nano **5**, 7108–7116 (2011). doi:10.1021/nn201808g

23. Xu, Q., Liu, F., Meng, W., Huang, Y.: Plasmonic core-shell metal-organicnanoparticles enhanced dye-sensitized solar cells. Opt. Express **20**, A898–A907 (2012). doi:10.1364/OE.20.00A898

24. Dang, X., Qi, J., Klug, M.T., Chen, P.-Y., Yun, S., Fang, N.X., Hammond, P.T., Belcher, A.M.: Tunable localized surface plasmon-enabled broadband lightharvesting enhancement for high-efficiency panchromatic dye-sensitized solar cells. Nano Lett. **13**, 637–642 (2013). doi:10.1021/nl3043823

25. Xiong, J., Li, Z., Chen, J., Zhang, S., Wang, L., Dou, S.: Facile synthesis of highly efficient one-dimensional plasmonic photocatalysts through Ag@Cu_2O core-shell heterononanowires. ACS

Appl. Mater. Interfaces **6**, 15716–15725 (2014). doi:10.1021/am502516s

26. Yang, J., Dennis, R., Sardar, D.: Room-temperature synthesis of flowerlike Ag nanostructures consisting of single crystalline Ag nanoplates. Mater. Res. Bull. **46**, 1080–1084 (2011). doi:10.1016/j.materresbull.2011.03.003

27. Sadeghi, B., Sadjadi, M., Vahdati, R.: Nanoplates controlled synthesis and catalytic activities of silver nanocrystals. Superlattices Microstruct. **46**, 858–863 (2009). doi:10.1016/j.spmi.2009.10.006

28. Nouneha, K.H., Oyama, M., Diaz, R., Abd-Lefdil, M., Kityk, I., Bousmina, M.: An approach to surface functionalization of indium tin oxide for regular growth of silver nano-particles and their optical features. J. Alloy. Comp. **509**, 2631–2638 (2011). doi:10.1016/j.jallcom.2010.11.172

29. Jia, H., Zeng, J., Song, W., An, J., Zhao, B.: Preparation of silver nanoparticles by photo-reduction for surface-enhanced Raman scattering. Thin Solid Films **496**, 281–287 (2006). doi:10.1016/j.tsf.2005.08.359

30. Zhu, Y.P., Wang, X.K., Guo, W., Wang, J.G., Wang, C.: Sono-chemical synthesis of silver nanorods by reduction of sliver nitrate in aqueous solution. Ultrason. Sonochem. **17**, 675–679 (2010). doi:10.1016/j.ultsonch.2010.01.003

31. Reicha, F.M., Sarhan, A., Abdel-Hamid, M.I., El-Sherbi, I.M.: Preparation of silver nanoparticles in the presence of chitosan by electrochemical method. Carbohydr. Polym. **89**, 236–244 (2012)

32. Zhang, X., Liu, J., Li, S., Tan, X., Yua, M., Dua, J.: Bioinspired synthesis of Ag@TiO2 plasmonic nanocomposites to enhance the light harvesting of dyesensitized solar cells. RSC Adv. **3**, 18587–18595 (2013)

33. Xiong, Y., Wu, H., Guo, Y., Sun, Y., Yang, D., Da, D.: Preparation and characterization of nanostructured silver thin films deposited by radio frequencymagnetron sputtering. Thin Solid Films **375**, 300–302 (2000). doi:10.1016/S0040-6090(00)01253-0

34. Alonso, J., Diamant, R., Castillo, P., AcostaeGarcía, M.C., Batina, N., Haro-Poniatowski, E.: Thin films of silver nanoparticles deposited in vacuum by pulsed laser ablation using a YAG: Nd laser. Appl. Surf. Sci. **255**, 4933–4937 (2009). doi:10.1016/j.apsusc.2008.12.040

35. Amiri, M., Nouhi, S., Azizian-Kalandaragh, Y.: Facile synthesis of silver nanostructures by using various depositionpotential and time: a nonenzymetic sensor for hydrogen peroxide. Mater. Chem. Phys. **155**, 129–135 (2015). doi:10.1016/j.matchemphys.2015.02.009

36. Pathan, H.M., Lokhande, C.D.: Deposition of metal chalcogenide thin films by successive ionic layer adsorption and reaction (SILAR) method. Bull. Mater. Sci. **27**(2), 85–111 (2004). doi:10.1007/BF02708491

37. Mitzi, D.B.: Solution Processing of Inorganic Materials. Wiley, New Jersey (2009)

38. Isah, K.U.: Successive ionic layer adsorption and reaction deposition of cadmium sulphide thin films. Nigerian J. Phys. **20**, 335–339 (2008)

39. Yu, B., Leung, K.M., Guo, Q., Lau, W.M., Yang, J.: Synthesis of Ag–TiO_2 composite nano thin film for antimicrobial application. Nanotechnology **22**, 1–9 (2011)

40. Hao, S., Wu, J., Huang, Y., Lin, J.: Natural dyes as photosensitizers for dye-sensitized solar cell. Sol. Energy **80**, 209–214 (2006). doi:10.1016/j.solener.2005.05.009

41. Cherepy, N.J., Smestad, G.P., Gratzel, M., Zhang, J.Z.: Ultrafast electron injection: implications for a photoelectrochemical cell utilizing an anthocyanin dye-sensitized TiO2 nanocrystalline electrode. J. Phys. Chem. B **101**, 9342–9351 (1997). doi:10.1021/jp972197w

42. Fernandez-Lopez, J.A., Castellar, R., Obon, J.M., Alrnela, L.: Screening and mass-spectral confirmation of betalains in cactus

pears. Chromatographia **56**, 591–595 (2002). doi:10.1007/BF02497675

43. Duran, E., Andujar, J.M., Enrique, J.M., Perez-Oria, J.M.: Determination of PV generator I-V/P-V characteristic curves using a DC-DC converter controlled by a virtual instrument. Int. J. Photoenergy **843185**, 1–13 (2012). doi:10.1155/2012/843185

44. Luan, X., Wang, Y.: Plasmon-enhanced performance of dye-sensitized solar cells based on electrodeposited Ag nanoparticles. J. Mater. Res. Technol. **30**, 1–7 (2014). doi:10.1016/j.jmst.2013.09.007

45. Berginc, M., Krašovec, U.O., Topic, M.: Solution processed silver nanoparticles in dye-sensitized solar cells. J. Nanomater **357979**, 1–11 (2014). doi:10.1155/2014/357979

46. Zaghouani, R.B., Manai, L., Rezgui, B.D., Bessais, B.: Study of silver nanoparticles electroless growth and their impact on silicon properties. Chem. J. **1**, 90–94 (2015)

47. Wen, C., Ishikawa, K., Kishima, M., Yamada, K.: Effects of silver particles on the photovoltaic properties of dye-sensitized TiO$_2$ thin films. Sol. Energy Mater. Sol. Cells **61**, 339–351 (2000). doi:10.1016/S0927-0248(99)00117-8

48. Ishikawa, K., Wen, C.J., Yamada, K., Okubo, T.: The photocurrent of dye-sensitized solar cells enhanced by the surface plasmon resonance. J. Chem. Eng. Jpn. **37**, 645–649 (2004). doi:10.1252/jcej.37.645